Colorimetric pH indicators based on well-defined amylose and amylopectin matrices enriched with anthocyanins from red cabbage

Marwa Faisal [a], Marta Bevilacqua [b,*], Rasmus Bro [b], Heloisa N. Bordallo [c], Jacob Judas Kain Kirkensgaard [b,c], Kim H. Hebelstrup [d], Andreas Blennow [a,*]

[a] Department of Plant and Environmental Sciences, Faculty of Science, University of Copenhagen, Denmark
[b] Department of Food Science, Faculty of Science, University of Copenhagen, Denmark
[c] Niels Bohr Institute, Faculty of Science, University of Copenhagen, Denmark
[d] Department of molecular Biology and Genetics, Aarhus University, 4200 Slagelse, Denmark

A B S T R A C T

This study aimed to prepare a novel colorimetric indicator film from virtually pure (99 %) amylose (AM) and anthocyanins extracted from red cabbage (RCA). The AM used was a unique engineered bulk material extracted from transgenic barley grains. Films produced by solution casting were compared to normal barely starch (NB) and pure barley amylopectin (AP), with amylose contents of 30 % and 0 %, respectively. The pH-indicator films were produced by incorporation of RCA into the different starch support matrices with different amylose contents. Barrier, thermal, and mechanical properties, photo degradation stability, and release behavior data revealed that RCA interact differently through the glucan matrices. Microstructural observations showed that RCA were evenly dispersed in the glucan matrix, and AM+RCA indicator films showed high UV-barrier and mechanical performance over normal starch. FTIR revealed that RCA was properly affected by the AM matrix. Moreover, the AM+RCA films showed sensitive color changes in the pH range (2–11) and a predominant Fickian diffusion release mechanism for RCA. This study provides for the first time data regarding AM films with RCA and their promising potential for application as support matrices in responsive food and other industrial biodegradable packaging materials.

1. Introduction

Current flexible food packaging does not fulfill the demands of providing information on the freshness of its contents, which is increasingly essential to secure safety during food transportation and storage. For many foods, especially protein-rich foods, there is a relation between food spoilage and the pH value of the food, mainly due to the production of organic acids, and ammonia during spoilage [1]. Hence, food freshness can be readily monitored by sensing the difference in the pH values of the food or of its headspace, which in turn can be visually specified using pH-sensing pigments in the packaging. Colorimetric pH indicators have shown potential in evaluating the freshness of food [2]. Such indicators typically consist of a solid support integrated with a pH-sensing pigment. Apart from its food safety characteristics, the support matrix must provide a molecular and physical environment for the sensor pigment, permitting stability and control diffusion. Natural polysaccharide polymers such as starch, chitosan, cellulose, and agar-

based gellan gum provide food-safe and inexpensive support matrices for the pH-sensitive pigment [3,4].

Typically, native starch is a granularly combined mixture of two types of polysaccharides, amylopectin (AP) and amylose (AM). The physio-chemical characteristics of the starch are fundamentally dependent on the relative content of these two polysaccharides [5]. Starch-based packaging is being developed to alleviate environmental pollution. Usually, starch consists of AM ranging from approximately 20–30 % and 70–80 % AP exhibits weak mechanical properties, and has a high moisture content, leading to water sensitivity and high solubility of the final polymer [6].

AM is a molecularly rather well defined starch polysaccharide showing very high mechanical strength [7] and lower kinetics during acid hydrolysis [8]. Films prepared with a higher amount of AM typically possess high mechanical strength, water resistance, and improved gas permeability [9]. However, protocols for isolating AM from starch, including AM leaching, precipitation, and electro sedimentation, are

* Corresponding authors.
  E-mail addresses: marta@food.ku.dk (M. Bevilacqua), abl@plen.ku.dk (A. Blennow).

suitable only for small-scale applications [10]. Recently, large quantities of pure AM could be obtained from a transgenic barley grain with suppressed starch branching enzyme activity [11]. This polysaccharide has been found to meet bioplastics requirements, also as a composite with nanocellulose [12]. Such AM, is a game changer for economically viable production as compared to the cumbersome post-harvest separation of AM from AP in normal starch.

Using pure glucan systems as raw materials for bioplastics is associated with shortcomings, such as brittleness, high moisture content, and poor cohesiveness. Plasticizing agents such as polyols (i.e., glycerol, xylitol, etc.) and organic acid crosslinking can overcome the brittleness and offer flexibility to the films [13]. Although high AM starches (HAS), such as Gelose 80 and HylonV, display better mechanical strength and water resistance, they do not offer ideal structures due to the presence of highly branched short chain segments of AP that form double-helical junction zones that produce weak mechanical properties and water-sensitive films [14,15]. HAS possesses a highly compact and dense structure with minimal voids. Starch granules undergo a complex process known as gelatinization, wherein they are suspended in water and heated to varying temperatures depending on the origin of the starch. Gelatinization is a crucial step in optimizing the processing of starch-based materials. HAS exhibits high thermal resistance, necessitating the application of higher temperatures to fully gelatinize it using high-pressure equipment like extrusion at 160 °C [16,17].

AM molecules have been suggested to perform act as "rods" that penetrate the granular matrix in a stable manner. Unlike AP double helices, which extensively hydrate and unwind, AM molecules are not easily hydrated and do not swell [18,19]. The gelatinization of HAS requires exceptionally high temperatures, which limits its applicability. However, this limitation can be overcome by employing specific thermal protocols such as high-pressure heating or microwave heating. Additionally, pretreatments like alkali treatment can directly gelatinize HAS or reduce the gelatinization temperature.

The gelatinization process of HAS appears to be more dynamic and complex compared to NB due to the interaction between AM and AP. Therefore, there is currently no straightforward explanation or available data regarding the thermal resistance of HAS, as discussed earlier [18].

Therefore, pure AM with an AM content of 99 % can be considered a leading solution as a raw material for bioplastics manufacturing. AM produced from AM-producing grain provides some unique properties as a support matrix for pH colorimetric indicators due to its non-toxicity, transparency, odorless, and ease of preparation.

Amylose, being a modified type of starch deposited in the grain, can extracted using well established, but further optimized, protocols. With a 20 % yield-loss in the grain as compared to normal starch, the costs as compared to starch are only marginally increased.

pH-indicators, including artificial pigments, have been used, such as bromocresol green [20], but their use in food applications is limited due to their environmental concerns [21]. Natural pigments derived from fruits and vegetables, i.e., red cabbage [22], carrot [23], and curcumin [24], provide better alternatives to artificial compounds when used in food systems.

Previous studies propose that anthocyanins can be suitable as color indicators to monitor pH-associated food spoilage. Factors like molecular structure, pH, temperature, the presence of co-pigments, and exposure to UV-light affect the color variations in anthocyanin. Anthocyanins from various sources have been used to improve real-time colorimetric indicators [22,25]. The anthocyanins extracted from red cabbage (RCA) are water-soluble pigments with high spectral stability at a rather wide range of pH-values due to the presence of the acylated group [26].

Analysis of anthocyanin-based films fabricated with normal cornstarch (AM 31 %) and cassava starch (AM 26 %) has shown that the anthocyanin increases the elongation at break and reduces the tensile strength of the starch of the support matrix. This phenomenon can be attributed to the presence of phenolic groups in the anthocyanin

structure, which act as plasticizers by decreasing interactions between polysaccharide segments [27].

We hypothesize that pure AM, produced in a transgenic crop, owing to its unique structure, is optimal for designing a mechanically strong and functionally solid support for a pH-indicator. This is the initial endeavor to prepare a pH-indicator from pure AM and RCA using a blending-casting protocol, which also possesses the potential to be scaled up industrially. Hence, for direct comparison, we introduced the RCA in differently structured support matrices encompassing the full range of AM-AP ratios, including normal barley starch (NB), pure amylopectin (AP), and pure amylose (AM).

Thermal, barrier, mechanical, and micro-structural properties, optical properties, photo storage stability, indicator release, and diffusion parameters were analyzed. Important differences for the three different glucan support matrices were found. Specifically, the AM matrix showed strong potential as a solid support for the preparation of functional pH-sensing films. AM+RCA-based pH-indicator systems not only offer high mechanical strength but are also of significant value for multifunctional biomaterials in many additional applications.

2. Materials and methods

2.1. Materials

Starch was extracted and purified from three barley genotypes: a control normal barley NB; a cultivar Golden Promise, which is a genetically modified AM-producing line produced by starch branching enzymes (RNA interference) in the Golden Promise background. AM recovery of AM extraction to achieve a 90 % pure amylose preparation was in average 50 % of the amylose in the grain, while >98 % pure amylose preparation was recovered at a 20–30 % recovery [15]. Pure AP (waxy) line derived from the cultivar Cinnamon kindly provided by Lantmännen, Sweden.

The molecular and physicochemical characteristics of the starch raw materials used in this study have been described in detail in earlier studies [7,8,28]. Anthocyanins (water-soluble) extracted from red cabbage were provided by Chr. Hansen A/S (Hørsholm, Denmark). Merck (Darmstadt, Germany) provided all other chemicals used.

2.2. Anthocyanin contents of red cabbage (TAC)

The total anthocyanin content of red cabbage (TAC) was estimated as described [23,29]. KCl (0.025 M, pH 1) and Na-acetate buffer (3.6 mL, 0.4 M, pH 4.5) were mixed independently into 0.4 mL of red cabbage pigment. The absorbance of both solutions was measured at 510 and 700 nm using a UV–Vis spectrophotometer (Biotech Synergy H1, USA), and the TAC was calculated as mg of cyanidin-3-glucoside/100 mL of RCA using Eqs. (1) and (2):

$$A = (A510 - A700) \, pH1 - (A510 - A700) \, pH4.5 \tag{1}$$

$$TAC = \frac{A \mathrm{x} MW \mathrm{x} 100}{MA} \tag{2}$$

Where A is the absorbance, MW is the molecular weight of cyanidin-3-glucoside (449.2 Da), and MA is its molar absorptivity (26900).

2.3. Preparation of films

2.3.1. Slurry film preparation and gelatinization

The starch-based film formulations were prepared as follows: 3 % of starch types with different amylose contents (AM), i.e., very high AP (0 % AM), normal starch (NB, 30 % AM), and very high AM (99 % AM) [15], were mixed with glycerol 30 % as a plasticizer. All the constituents were stirred while being heated for 30 min at 100 °C for AP and 140 °C for NB and AM, using a high-pressure glass reactor. The solutions were cast immediately in Teflon-coated petri dishes after cooling to 70 °C. The films were dried at 40 °C in an aerated oven until complete dryness.

2.3.2. Preparation of pH-indicator films

The total anthocyanin content (TAC) was 8 mg/100 mL. Our primary results showed that a lower concentration of RCA, when incorporated in a 3 % AM solution, was not suitable for the development of the indicator due to the narrow changes in the color of the indicator in the pH-buffer solutions. 0.1 g of RCAs were added to the gelatinized 3 % starch solution at 40–50 °C to avoid RCA degradation and stirred for 10 min. The mixtures were poured into Teflon-coated Petri dishes and dried in an oven at 40 °C. To equilibrate the moisture content before experimental analysis, all films were kept in an airtight desiccator saturated with KCl (RH 65 %, 20 °C). Control starch films devoid of RCAs are denoted AP, NB, and AM, and films containing RCAs are denoted as AP + RCA, NB + RCA, and AM+RCA.

2.4. Characterization of indicator films

2.4.1. Moisture content

The water content of the films was determined according to [30], using a gravimetric protocol. Film samples (2x2 cm) were placed in an oven at 105 °C for 24 h. The moisture content was calculated (Eq.3):

$$MC(\%) = (initail\ weight - final\ weight) \times 100 / _{(initail\ weight)} \tag{3}$$

2.4.2. Solubility in water

Total soluble matter was analyzed as described by [31]. Films (2 × 2 cm) were submerged in MilliQ water (50 mL), and introduced to the shaking incubator (ES20 Benchtop shaking incubator, BIOSAN, Latvia) at 120 rpm and at room temperature (25 ± 2 °C) for 24 h. Then the films were taken out from the solution and set in an oven at 105 °C for 24 h to achieve complete dryness. The initial weight was evaluated considering the initial water content of the sample. Finally, the solubility of the films in water was calculated using Eqs. (4, 5, and 6):

$$Initial\ dry\ weight = W1 \times (1 - MCWb) \tag{4}$$

$$Final\ dry\ weight = W3 - W2 \tag{5}$$

$$Solubility\ (\%) = ((Initial\ dry\ weight - Final\ dry\ weight)\ /\ Initial\ dry\ weight\ ) \times 100 \tag{6}$$

2.4.3. Fourier transform infrared (FTIR) spectroscopy

The FTIR analysis of the film samples was measured using a Bomem MB100 FTIR spectrometer (ABB-Bomem, Quebec, Canada), with an attenuated total reflectance (ATR) single reflectance cell and a diamond crystal. The samples were scanned 64 times over the range of 4000–600 cm^{-1} at a resolution of 4 cm^{-1} against air as the background. From the FTIR spectra, chemical interactions between the matrices and natural fillers were distinguished. Each sample was scanned twice, and reproducibility was secured.

2.4.4. Wide-angle X-ray diffraction (WAXS)

WAXS analysis of the film was conducted on a Nano-inXider instrument from Xenocs (Grenoble, France) using a Cu Kα source with a 1.54 Å wavelength and a 2D 300 K Pilatus detector (Dectris Ltd., Baden, Switzerland). Samples were placed between mica windows, and background contributions were deducted from the measured spectra. The relative crystallinity (RC) of the peaks was calculated as the ratio of the crystalline reflexions area to the whole diffraction area via Peak Fit software (Version 4.0, Systat Software Inc., and San Jose, CA, USA).

2.4.5. Thermogravimetric analysis (TGA)

TGA coupled to FTIR was used to describe the thermal stability of the films. All films were analyzed using TG 209 F1 Libra PERSEUS from NETZSCH attached to an FTIR (Bruker Optics) at an N$_2$ atmosphere (20 mL/min) and a heating rate of 10 K/min. Samples were placed in an Al$_2$O$_3$ crucible with an automatic sample changer, and a temperature ramp of 28 °C to 600 °C and instrument correction were performed on an empty crucible. The data were handled by software from NETZSCH. The FTIR spectra of the produced gases were verified for every 3 °C. Based on the TGA data, FTIR spectra were selected at temperatures of interest, and further evaluated.

2.4.6. Water vapor permeability (WVP)

WVP was tested [12,32]. Films were placed in a sealed dissector for five days at 85 % RH to secure humidity equilibrium. Round disks, 5 cm in diameter were measured at 25 °C at 85 % RH in duplicate.

2.4.7. Mechanical measurement

The thickness of each film was analyzed in five replicates with a micrometer device (148–121 Zhongtian Experimental Instrument Co., Ltd., China). A TA-XT plus texture analyzer (TTC Company, UK) with a grip accessory and a 30 kg load cell analyzed the tensile tests of the starch films (5 × 40 mm strips equilibrated at 67 % relative humidity at 22oC for 5 days). The parameters (Young's modulus, tensile strength, and elongation to break) were computed from stress-strain curves. Data for each sample was created on 5–7 replicates [33].

2.4.8. Field emission scanning electron microscopy (FE-SEM)

FE-SEM images were produced with a Quanta 3D FEG (FEI Company, The Netherlands) on film specimens (1 × 1 cm), mounted onto a metal plate, and sputtered with colloidal gold. Cross-section morphology was imaged following cryo-fracturing in LiqN$_2$ [12].

2.4.9. Opacity and light barrier properties

UV/Vis light barrier was examined [34] on film sections (3 × 3 mm) in an UV–Vis spectrophotometer (BioTeK Synergy H1, USA), so that the light beam passed through the film surfaces. The wavelengths of transmittance between 200 and 800 nm were measured in triplicate. The opacity of the films was measured at 600 nm and calculated (7):

$$Opacity = \frac{Absorbance\ at\ 600\ nm}{Thickness\ of\ the\ film} \tag{7}$$

2.4.10. Color spectra of the pH-indicator films at different pH

Film color parameters were obtained by using the multispectral imaging device Video meter (Video meter A/S, Denmark). Through this instrument, a multispectral image of each sample placed under its dome is acquired using specific and constant lightning settings. This allows the possibility of recording several (18 in particular) wavelengths in the Vis-NIR spectral region (from 450 to 950 nm) on each pixel of each sample in a few seconds.

Films (2 × 2 cm) containing anthocyanins prepared with the three different types of starch were immersed in different buffer solutions ranging in pH 2–11. For each sample, the films were immersed for 5 min, the liquid was removed, and the sample (in triplicate) was placed under the dome of the imaging spectrometer over a standard white background. An extended region of interest (ROI) was then extracted from each image recorded, and all the pixels in this region were averaged to obtain for each sample a multi-wavelength spectrum that was representative of the whole film.

The data were in terms of the following color parameters: L* value (lightness; 0; pure black; 100; pure white); chroma a* (greenness to redness); and chroma b* (blueness to yellowness).

To do so, a set of colorful calibration samples that were earlier analyzed (in triplicates) on a Minolta CR-300 colorimeter (Konica Minolta, Japan) for their L*a*b* parameters were also measured with the same multispectral imaging device using the same illumination settings as for the samples. Through a multivariate calibration procedure using a partial least squares PLS model [35], the spectral characteristics of each film could then be expressed in terms of their L*a*b* values. The total color difference (ΔE) was measured (Eq. 8):

$$\Delta E^* = (L^* - Lo) + (a^* - ao) + (b^* - bo)^{1/2} \qquad (8)$$

where values of L*, a*, and b* denote the color parameters obtained on each sample at different pH, and L_o, a_o, and b_o correspond to the color parameters of the indicator film in its normal form before immersion in the buffer media [25].

2.4.11. Photo degradation of RCAs during storage

Photo degradation of RCA in films was investigated by keeping the three films containing RCA under constant visible light irradiation. Two series of similar square samples (2 x 2 cm) of each kind of film (three replicates for each film) were kept in a closed cabinet with constant humidity (32 %) and temperature (25 °C) for a total of 35 days. One series was kept under standard lighting conditions (750 Lux-LED lamp, white), while the other series was kept in the same cabinet but kept in complete darkness to be used as a control. The samples were analyzed daily to obtain their color parameters, using the same procedure as in Section 2.4.10.

2.4.12. Release behavior of RCA

RCA release from the films was assessed using a solution of acetic acid (3 %) as a food simulant, as described [36] with some modifications. A series of 250-mL Erlenmeyer flasks (containing 100 mL of 3 % aqueous acetic acid and specimens sized 4 × 4 cm) were put in a shaker (100 rpm, 25 °C), and kept in the dark. During the incubation, the absorbance of the solutions was measured periodically at 540 nm. To retain the total volume constant, the solutions were immediately returned to their original flask. The RCA release was determined based on linear regression (Fig. S5), and the accumulative release was calculated using Eq. (9):

$$Accumulative\ release(\%) = \left(\frac{Mt}{Mo}\right) \times 100 \qquad (9)$$

The amount of RCA define anthocyanin released from films at time *t* is defined as M_t *(mg)*, and the total amount of RCA integrated in films is expressed as M_o (mg). The release behavior of RCA was calculated as described in [37], and expressed in Eq. (10):

$$\frac{Mt}{M\infty} = kt^n \qquad (10)$$

The amount of RCA released at time *(t)* corresponds to M_t (mg), and the amount of RCA released at equilibrium corresponds to M_∞ *(mg)*; *k* is the rate constant of the process, and n is the release exponent n (revealing of the type of the release mechanism). When n is equal to 0.5, Fickian release behavior dominates, and the following approximation of Fick's second law of diffusion is used (Eq. (11)) for short times (for $M_t/M_\infty \leq 0.6$):

$$M_t/M_\infty = 4\left[\frac{Dt}{\pi l^2}\right]^{1/2} \qquad (11)$$

Where *D* denotes the diffusion coefficient of the RCA and *l* the thickness of the film. For a Fickian release behavior, the diffusion coefficient *D* can be derived from the rate constant, k, according to Eq. (12):

$$k = 4\left[\frac{D}{\pi l^2}\right]^{1/2} \qquad (12)$$

The additional five classic models: $M_t/M_\infty = kt$ (zero-order), $(1 - M_t/M_\infty) = kt$ (first-order), $Mt./M_\infty = kt/(1+kt)$ (second-order), $(1 - Mt/M_\infty)^{1/3} = -kt$ (Hixson-Crowell), and $M_t/M_\infty = kt^{1/2}$ (Higuchi), were verified to fit the experimental data.

2.5. Statistical analysis

Solubility, thickness, moisture content, photodegrading data, barrier properties, thermal properties, and mechanical properties were statistically calculated with analysis of variance (ANOVA) and Tukey's test HSD post hoc test of IBM SPSS Statistics at 95 % confidence level or significance level of 0.05 (*p*-value).

The color parameter results were then analyzed by two-way ANOVA (two factors: pH and the type of α-glucan film), using a multivariate linear model on pH = 2–11; AM+RCA, NB + RCA, and AP + RCA, respectively. Tukey's HSD was employed with a significance level α = 0.05, using IBM SPSS Statistics. The release behavior data analysis was done in a Matlab environment, version R2020a (The Math Works, Inc., USA), using both the PLS_toolbox (Eigenvector Research, Inc., USA) and in-house written routines.

3. Results and discussion

3.1. Physical characteristics of the films

The AM films had the least solubility compared to the AP and NS films (Table 1), due to the high content of AP chains that increase hydrophilic properties. Films with RCA increased the water solubility in the following order: AP + RCA > NB + RCA > AM+RCA. This behavior is likely an effect of the high amount of hydrophilic groups made available for water absorption following hydrophobic interaction between the RCA and AP parts of the starch films. Such hydration, is caused by RCA disruption and discontinuity of the polymer matrix, resulting in water solubilization of the films [38,39].

Control films showed higher moisture contents than the films with RCAs due to the abundance of hydroxyl groups in the RCA increasing intermolecular hydrogen bonding with the hydroxyl groups in starch. AP films had a higher water content capacity, indicating a high hydrophilicity as compared to the NB and AM films. In previous studies [40,41], the moisture content of starch films with anthocyanins extracted from Russian box thorn (*Lycium ruthencium)* films significantly decreased with increasing anthocyanin content compared to starch films. Similar results were shown for anthocyanins extracted from Roselle (*Hibiscus sabdariffa*) and starch/polyvinyl alcohol films due to the interactions between RCAs and starch/polyvinyl alcohol, which reduced the hydroxyl groups of starch to interact with water [30].

3.2. FTIR spectroscopy

FTIR can detect possible interactions in polymeric blends (Fig. 1). The spectrum of RCAs has typical bands at 3300 cm^{-1} (OH stretching), 1646 and 1514 cm^{-1} (C—C stretching bands), 1336 cm^{-1} (aromatic ring C=O), and 1019 cm^{-1} (deformation of the aromatic ring C—H). All starch films showed the same characteristic peaks: broad bands at 3310 cm^{-1}, 2927 cm^{-1}, 1645 cm^{-1} and peaks from 1016 to 927 cm^{-1} (C-O-C stretching). Any apparent band shift or perceptible new peak in the FTIR spectra with any component specifies interaction within the components. A new small peak around 1514 cm^{-1} appeared in AP + RCA, NB + RCA, and AM+RCA, which was related to the overtones of aromatic compounds, verifying that RCAs have been incorporated into the starch matrix [42] (Fig. 1).

Table 1
Solubility, moisture content, measurements of the films.

Films	Film solubility in water (%)	Moisture content (%)
AP	45.6 ± 5.0[c]	34.6 ± 10.6[b]
NB	17.9 ± 10.5[a,b]	19.3 ± 3.9[a,b]
AM	12.6 ± 10.4[a]	19.1 ± 7.5[a,b]
AP + RCA	50.3 ± 4.4[c]	5.6 ± 1.2[a]
NB + RCA	31.0 ± 1.0[a-c]	6.0 ± 0.5[a]
AM+RCA	32.8 ± 6.0[b,c]	6.2 ± 1.4[a]

Mean values are given as ± SD (*n* = 3). Different letters the same column show significance difference (p < 0.05).
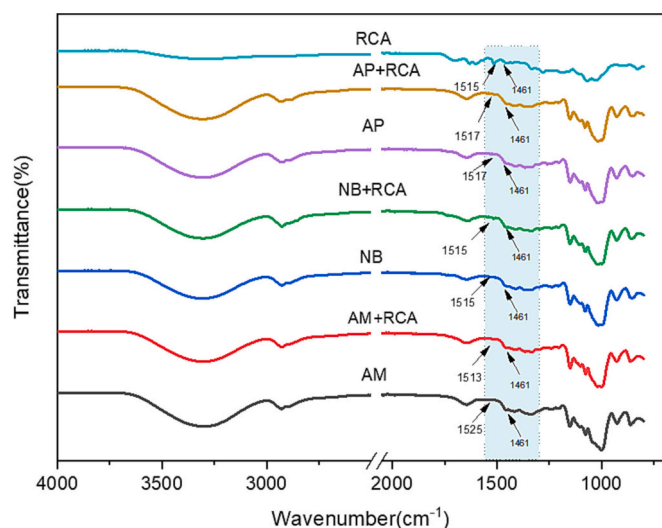
Fig. 1. Infrared spectrum of starch-based films with and without RCA.

Fig. 2. Crystalline diffraction (WAXS) of films with and without RCA.

FTIR has been used to evaluate the short-range order, such as helical motifs and chain conformation [35]. The ratio of absorbance at 1045 and 1022 cm^{-1} was used to describe the structure order of starch affected by RCAs (Table 2). The incorporation of RCA resulted in a reduction of the short-range order of the AM films, yielding a lower 1045/1022 cm^{-1} ratio. Thus, AM double helices and self-assembly in AM were hindered by the addition of RCA [43,44].

3.3. Crystalline properties of starch—RCA films

The intermolecular interaction between starch films and anthocyanin was also studied by WAXS. The WAXS profile of RCAs exhibited a big broad band at 2θ at 23° (Fig. 2). The NB and AM films showed a combined V-type crystalline polymorphic structure with well-defined reflections at 2θ values around 13°, 16.9°, 19.7°, 22°. Incorporation of RCAs did not change this scattering. This indicates that RCA is well dispersed in the matrix [45]. There was significant dissimilarity in the relative crystallinity (RC) among the starch films. The AM film showed the highest RC among all films before and after adding anthocyanins, while AP showed no crystallinity. The RC decreased significantly ($p <$ 0.05) in AM+RCA films (Table 2).

3.4. Thermal and decomposition characteristics

The TGA curves (Fig. 3a) characterize three mass loss regions. The critical point in the TG curves was recognized in the first temperature at each region. Based on starch films, the first stage exposed to 5–8 % mass loss between 40 and 120 °C was due to water loss from the samples. For the NB and AM films, a substantial weight loss around 235–375 °C was observed, as an effect of evaporation of glycerol and breakdown of starch, with maximum mass loss 54 % and 46.4 % at 306 °C and 302 °C respectively. However, the evaporation of glycerol and decomposition of starch occurred independently in AP films; the main degradation was
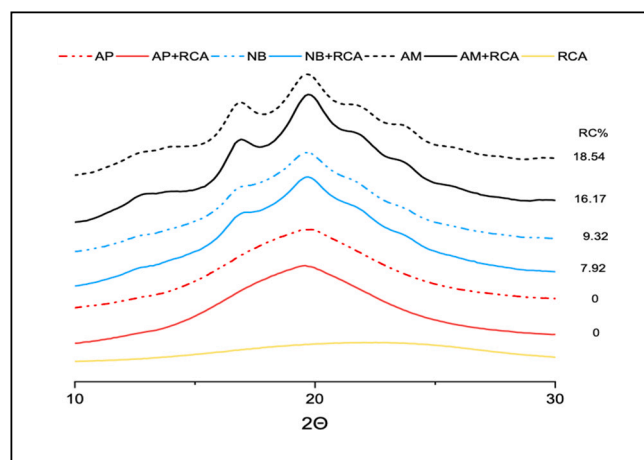
observed at around 130–200 °C, and the latter was observed around 240–370 °C with a maximum mass loss of 53 % at 308 °C (Table 2).

AM content did not significantly influence the thermal properties of the films. These results are also in agreement with the data reported by [46].

RCAs are thermally unstable and, hence, strongly affected by temperature. Pyrolysis of RCAs was previously reported, where the first thermal degradation starts at 130 °C and the second at 200 °C, where esters and CO_2 are released, while at 210–270 °C aromatic compounds, aldehydes, and ketones are formed. The pyrolysis of RCAs slows down above 300 °C and the main product is CO_2 [47]. Other studies reported that the maximum mass loss for blueberry anthocyanins occurred at 130 °C, due to its degradation to aldehydes and phenolic acid by deglycosylation [48]. Our data showed that the addition of RCAs to the films resulted in lower thermal stability in NB + RCA and AM+RCA films. Both films exhibited three steps of thermal degradation. For the NB + RCA films, the second decomposition phase was at 150–255 °C with a mass loss of 9 % due to the decomposition effect of anthocyanins, while the third decomposition was at 240–425 °C with a maximum mass loss of 49.4 % at 305 °C. The second degradation of the AM+RCA films was at around 130–240 °C with a mass loss 16 % at 180 °C and the third weight loss occurred from 240 to 325 oC with a maximal weight loss of 44.5 % at 293 °C. The addition of RCA significantly decreased the maximum degradation temperature of AM from 302 °C to 292 °C (Table 2). This can be attributed to the hydrogen bonding between the starch and phenolic compounds in the RCA, which agreed with the FTIR results, leading to the plasticization of the polymer matrix.

Similar results were reported by [43], suggested that this behavior was due to the non-uniformity of the AM+RCA interaction detected from the dynamic complexation process to achieve a thermodynamic equilibrium, which is typical for most structuring mechanisms of starch-based systems. The AP + RCA films showed higher thermal stability, with maximum mass losses of 44 % at 306 °C. Overall, the results indicated that all films have thermal stability until 50 °C and are thus stable enough to be safely efficient in the food industry.

Table 2

FTIR peak ratio, relative crystallinity (RC %), derivative thermogravimetric (DTG) and water vapor permeability measurements of the films.

Films	FTIR Peak ratio 1047/1022	Relative crystalinity RC%	DTG Peak Temperature (° C)	WVP × 10^{-10} (g mm^{-1} Pa^{-1} day^{-1})
AP	0.3 ± 0.0 [a]	0.0 ± 0.0 [a]	308.0 ± 2.3 [b]	4.9 ± 0.5[a,b]
NB	0.4 ± 0.0[a]	9.3 ± 0.3 [b]	306.3 ± 0.7 [b]	4.8 ± 0.4[a,b]
AM	1.8 ± 0.1[c]	18.5 ± 0.2 [d]	302.6 ± 2.6 [b]	7.9 ± 1.2[c]
AP + RCA	0.4 ± 0.1 [a]	0.0 ± 0.0 [a]	306.2 ± 1.4 [b]	6.2 ± 0.0[b,c]
NB + RCA	0.4 ± 0.0[a]	7.9 ± 0.8[b]	305.7 ± 0.8 [b]	3.7 ± 0.1[a]
AM+RCA	1.0 ± 0.1[b]	16.2 ± 0.7 [c]	292.7 ± 0.9 [a]	6.8 ± 0.1[b,c]

The data (mean ± SD) $n = 3$. Different letters denote significant difference ($p < 0.05$).
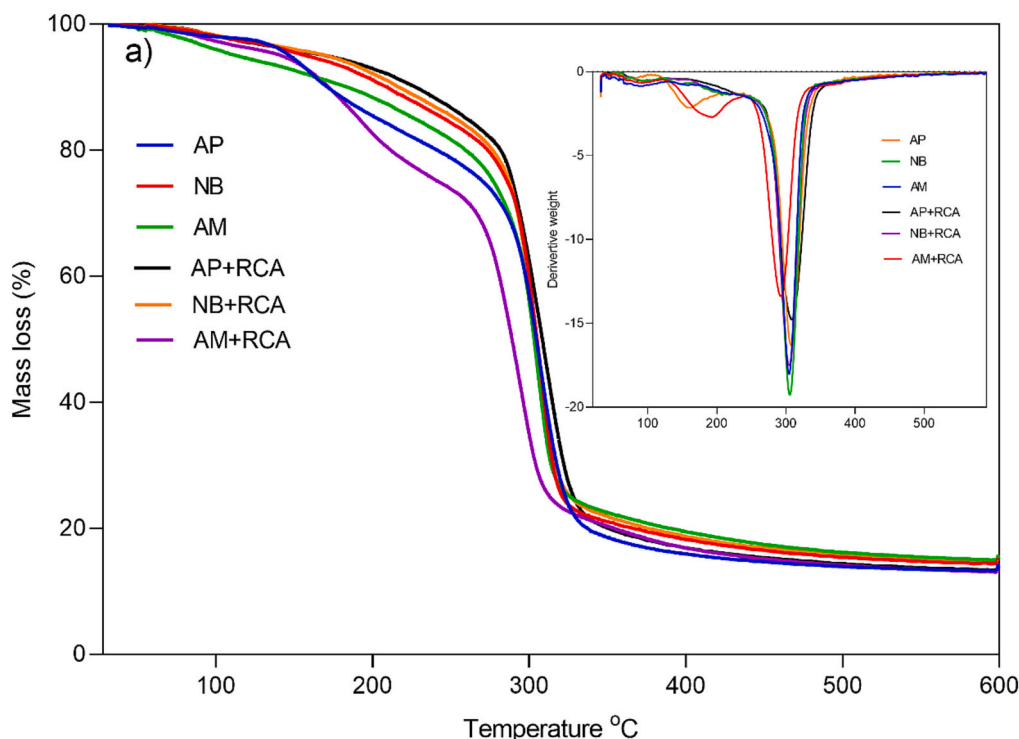
Fig. 3. Thermogravimetric analysis (TGA) and derivative thermogravimetric (DTG) of starch-based films with and without RCA.

Analysis of the infrared spectra of the decomposition gases was performed to understand the thermal decomposition mechanism (Fig. S1). Under a nitrogen atmosphere, the starch remained unchanged up to 275 °C and only water and glycerol losses were detected. At 300 °C, the decomposition of starch began (Fig. S2). Vibrational bands assigned to water (3605 cm^{-1}), carbon dioxide, and carbon monoxide (2327 and at 666 cm^{-1}) indicated molecular chain breakage in the range 300–334 °C. The observation of a vibration at 1743 cm^{-1} shows the production of new compounds, probably aldehydes [47].

The TG-FTIR spectra of the indicator films with RCAs showed no significant spectral difference between the AP + RCA and NB + RCA films. AM+RCA film was different from pure AM films in that the absorption band at 1054 cm^{-1} increased, which corresponds to C–O–C. AM showed lower intensity at 2350 cm^{-1}, which corresponds to CO_2 gas [47].

3.5. WVP

WVP should be reduced, as one of the main desired properties of a food packaging is to avoid, or at least decrease, the transfer of moisture between the food and the adjoining atmosphere. WVP depends on many parameters, including film structure, temperature, relative humidity, thickness, the crystalline fraction and added plasticizer. The AM films showed higher WVP than the AP and NB films (Table 2), which might

related to the high thickness of AM film (Table 3). It was confirmed by other studies that AP and AM ratios have a significant influence on WVP [49,50].

This result was in accordance with a study reporting that lower amylose content (28 %) showed lower WVP values than a (70 %) higher amylose content. This effect could be attributed to the fact that the AM results in increasing the free volume of the matrix, leading to higher diffusivity and increased WVP [51]. Our WVP results agreed well with the higher degree of crystallinity (Table 2).

The WVP of the films was not notably ($p > 0.05$) changed after including the RCA, which in accordance with the moisture content results (Table 1). This effect is likely due to low amount of RCA used in our study and the lack of disruption by the RCA of the network of the film matrix. The WVP was same as the moisture content trend, which can be related to the hydrogen bonds in the film matrix.

Similar results were observed by Góes et al. [52] with different plasticizers, in which glycerol-plasticized starch films showed unchanged WVP values after adding 10 ml of the anthocyanins extracted from grape skin (GSE) in 3 % of cassava starch film. Reporting that the lower water affinity of those films was suggested to be due to hydrogen interactions between phenolic compounds present in GSE and the starch, forming a dense and compact network that reduced the availability of hydroxyl groups to interact with water.

Table 3
Mechanical properties of starch-based films with and without RCA.

Samples	Young's modulus (GPa)	Tensile strength (MPa)	EAB (%)	Thickness (mm)
AM	0.52 ± 0.2[b]	10.8 ± 1.9[c]	7.6 ± 3.2[b]	0.2 ± 0.0[c]
NB	0.28 ± 0.1[b]	3.4 ± 0.6[a]	3.1 ± 1.2[a]	0.1 ± 0.0[a]
AP	0.03 ± 0.0[a]	1.4 ± 0.6 [a]	25.8 ± 0.1[c]	0.1 ± 0.0[a]
AM+RCA	0.43 ± 0.1[b]	5.7 ± 1.5[b]	7.9 ± 0.6[b]	0.2 ± 0.0[b,c]
NB+RCA	0.10 ± 0.0[a]	2.23 ± 0.0[a]	20.7 ± 0.1[c]	0.1 ± 0.0[a]
AP+RCA	0.01 ± 0.0[a]	0.52 ± 0.2[a]	21.9 ± 6.4[c]	0.1 ± 0.0[a,b]

Different letters represent values that are significantly different ($p < 0.05$).

3.6. Film microstructure

The cross section of starch films containing and devoid of RCA was investigated with FE-SEM (Fig. 4). Both the films with and without RCA had a compact and smooth cross-section morphology, which indicates biocompatibility and interaction between starch and RCA. Similar behavior was observed for anthocyanin starch and anthocyanin PVA composite, which was ascribed to excessive hydrogen electrostatic bonding between anthocyanin, starch, and PVA [30].

For the surface structures, the AM films without RCA showed more uniform and pleated surfaces, while the AP films showed the highest roughness (Fig. S3). The RCA-containing films, especially the AP matrix, had relatively smoother surfaces, characteristic of forming ordered, dense, and continuous molecular networks. This effect can be due to new bonds formed between RCA and starch. No agglomeration was found at the surface.

3.7. Mechanical properties

Functionality of starch-anthocyanin pH-indicator films depended on the amylose content. Anthocyanins in the films primarily affected the amylose in the film matrix. Tensile strength, Young's modulus, and elongation at break (EAB) data demonstrated that the Young's moduli and the tensile strengths of the AM film were 0.52 GPa and 10.8 MPa, respectively, which were higher and relatively stronger than the ones for the NB and AP films (Table 3). Similar behaviors have been detected in other studies, reporting that the larger moisture content in the films exert a plasticizing effect which increases the EAB and reduces the mechanical resistance [53,54].

The presence of the phenolic group in the RCAs potentially disrupts macromolecular interactions acting as plasticizers, decreasing the Young's moduli and tensile strengths of all the films.

The pure AM and AP matrices failed to demonstrate significant EAB, which likely an effect of the strong interaction between phenolic compounds in RCA and the starch [52], while it increased significantly ($p <$ 0.05) in NB+ RCA (Table 3), where. RCA caused the disordering of the starch matrix and resulted in an increase in EAB [30]. A similar behavior was observed in starch poly vinyl alcohol (SPVA) films added with glycerol, where the anthocyanins improved the compatibility of the starch and PVA so that the films became more homogenous, which resulted in enhanced extensibility [30].

AM has a thicker film (Table 3), it is well known that starch contains lower amount of AM would result in thinner film [46].The higher thickness is related to the higher viscosity of AM film-forming suspension (the results for viscosity are not presented in this paper) [55]. There was no significant difference in thickness results before and after RCAs incorporation in the films (Table 3).

3.8. Light barrier characteristics of the films

Protecting the food against light is an essential property of the packaging material, as light can result in photo deterioration for various components of the food that can be subtle at different light wavelengths. Hence, to evaluate the light barrier properties, the spectra of the starch films in the whole UV–vis region (200–800 nm) were investigated (Fig. S4).

Transmittance and opacity are influenced by the thickness and origin of starch, primarily the AP/AM ratio, molecular size, branching patterns, and the film preparation procedure. For instance, potato starch films demonstrate greater transparency compared to wheat films owing to the distinctive molecular structures of potato starch. Films lacking RCA exhibited higher transmittance than those with RCA. The transmittance order of these films was AP > AM > NB. Ortega-Toro et al. [52] presented similar findings, suggesting that films with more uniform
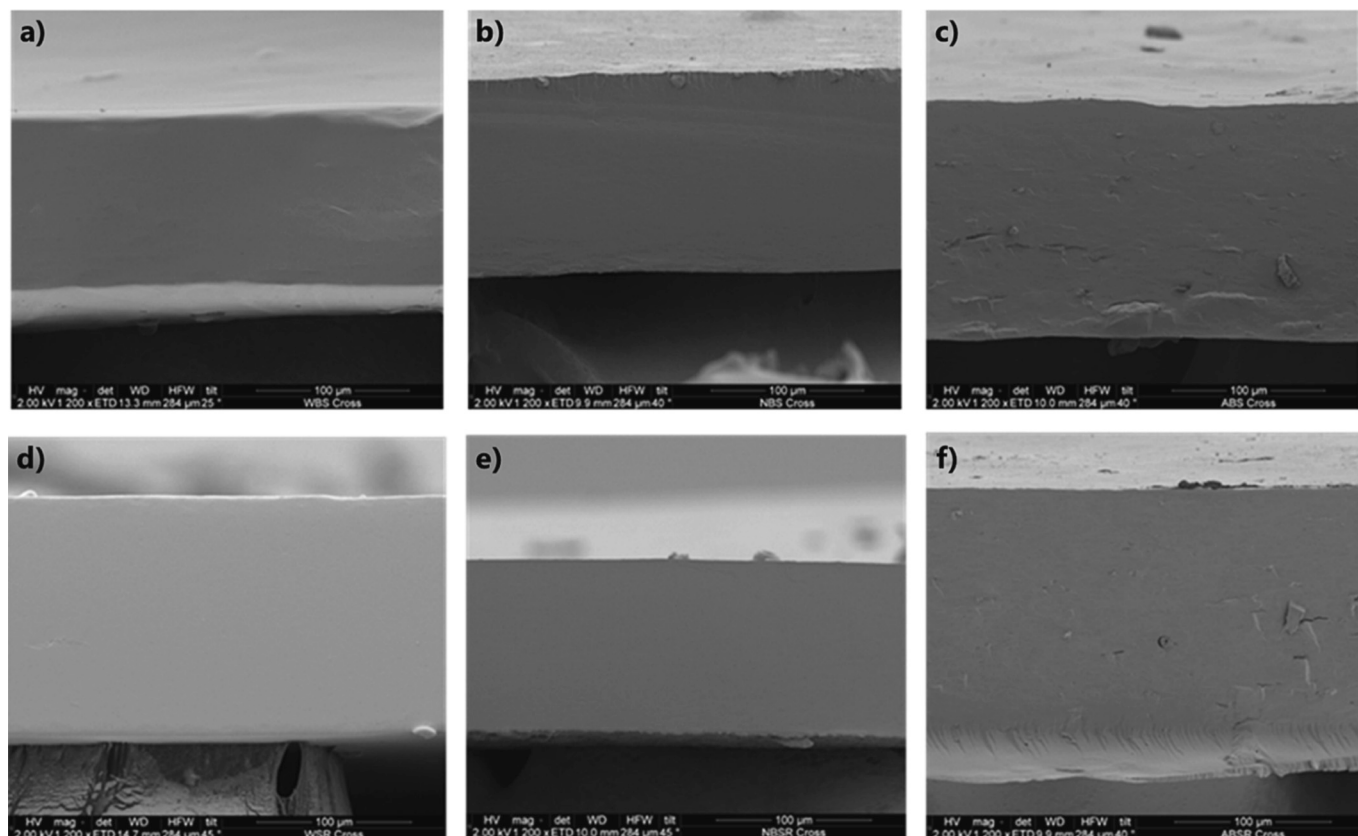
Fig. 4. FE-SEM of cross section of films a) AP, b) NB, c) AM, d) AP + RCA, e) NB + RCA, f) AM+RCA.

matrices (pure AM or pure AP) were more transparent. Furthermore, starch with a higher AP content is anticipated to possess greater transparency due to its increased hydration capacity.

Bertuzzi et al. [56] have reported similar findings, indicating that the formation of an elongated arrangement of amylose molecules in an alkaline environment promotes the development of a crystalline structure within the film matrix. This leads to a reduction in absorbance and an increase in film transparency. Additionally, the relatively shorter segments of AP also contribute to the transparency of the film. However, AM exhibited higher transparency than NB (Fig. S4). This effect may be attributed to the more crystalline regions exist in AM film increase the transmittance, while NB film has lower crystalline region which reduce the transmittance of light [57].

The RCA-containing films showed notably lower values than without RCA-films in the UV region (below 600 nm), while still presenting the same differences in transmittance between the different films: AP + RCA > AM+RCA > NB + RCA (Fig. S4). This may be described by the traces of different RCA structures such as phenolic acid, flavonoids, etc. that contain delocalized bonding arrangements absorbing in the UV/visible region [58].

As demonstrated by their high transmittance values, AP and AM showed lower opacity than NB. Adding RCA increased the opacity for all the film types, retaining the same order of opacity: NB + RCA > AM+RCA > AP + RCA (Table S1).

3.9. Colorimetric analysis of the films

Immersing the films in the different buffer solutions at pH 2–11 resulted in stabilized color within a few min (Fig. 5b). Color variations of anthocyanins with pH are directly related to alterations in the molecular structure of anthocyanins. Under acidic conditions (pH 1–3), the dominant form is the flavylium cation, which corresponds to the red and purple colors. At pH 4–5, the pseudo-base carbinol is dominating, which an effect is caused by the molecule's hydration. By increasing the pH to 6–7, the quinoidal basic purple structure prevails. The central ring opens, forming a yellow-colored chalcone structure at a higher pH of 8–9.

The trend of the film color changes was similar for all three polymers, gradually changing from red (pH 2–3) to purple (pH 4–7) and then to dark green (pH > 8). The AM+RCA films took less time (1 min) for color stabilization than the NB + RCA and AP + RCA films. The color parameters L*, a*, b*, and ΔE, were calculated for the various films (Section 2.4.10).

All films exhibited an increase in brightness (L*), going from pH 2 to 11. In particular, for all the films, the statistical difference in the L* value was non-significant or very mildly significant for pH ranges 2–8, while higher (statistically significant) increases were observed going from pH 8–9 and then from pH 9–10. For each given pH, the difference in L* between the three different films was mostly non-significant (Table 4).

For all the films, the chroma a* value decreased (46.3 to 20.8) as pH increased (2–11) due to the dominant chalcone structure at higher pH (Fig. 5b). Comparing the three films, the main statistical difference is a
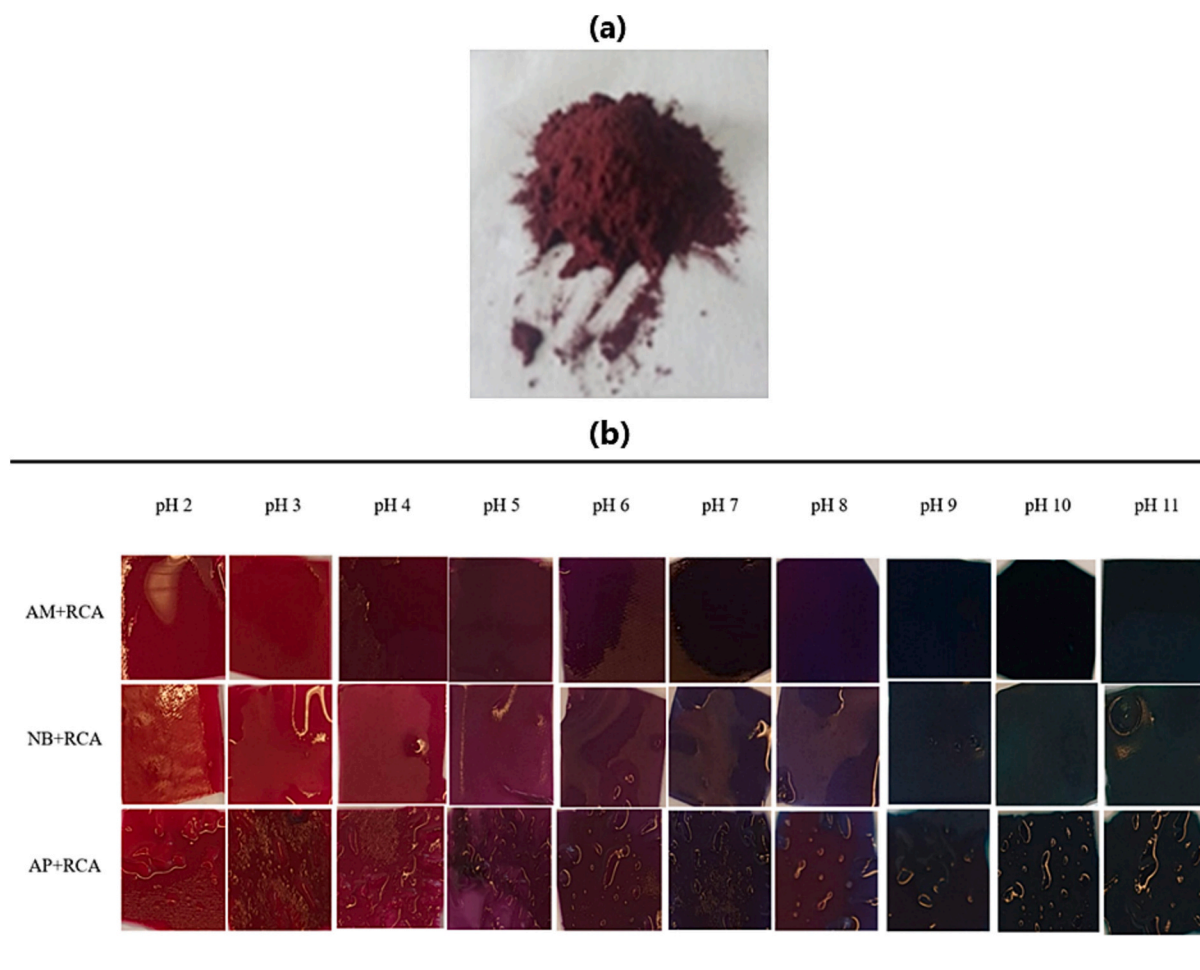
Fig. 5. a) Color of RCA powder used in the films, b) color changes of the Films after immersing indifferent buffer solutions (pH 2 to 11).

Table 4
Color parameters in different pH solutions.

Film	pH	L	a	b	ΔE
AM+RCA	2	33.9 ± 0.1$^{a/x,y}$	46.3 ± 0.8$^{f/x}$	0.1 ± 0.4$^{f/y}$	3.8 ± 0.6$^{a/x}$
	3	34.1 ± 0.1$^{a/x,y}$	46.3 ± 3.3$^{f/x}$	−0.7 ± 0.0$^{f/y}$	4.2 ± 1.8$^{a/x}$
	4	34.2 ± 0.4$^{a/x,y}$	36.6 ± 0.5$^{d,e/x}$	−1.3 ± .8$^{d/y}$	7.5 ± 0.7$^{a/x}$
	5	34.5 ± 0.1$^{a/x,y}$	35.0 ± 1.7$^{c/x}$	−3.6 ± 1.3$^{c/y}$	9.1 ± 1.5$^{b/x}$
	6	34.5 ± 0.4$^{a/x,y}$	35.5 ± 1.9$^{c,d/x}$	−5.6 ± 1.0$^{a,b/y}$	9.1 ± 1.5$^{b/x}$
	7	35.1 ± 0.3$^{b/x,y}$	29.9 ± 0.8$^{b/x}$	−5.4 ± 1.4$^{a,b/y}$	14.4 ± 0.5$^{c/x}$
	8	34.6 ± 0.4$^{a,b/x,y}$	33.9 ± 1.5$^{c/x}$	−7.2 ± 1.1$^{a/y}$	11.2 ± 0.1.0$^{c/x}$
	9	36.2 ± 0.2$^{c/x,y}$	24.7 ± 0.4$^{a/x}$	−3.9 ± 0.6$^{c/y}$	19.3 ± 0.4$^{e,f/x}$
	10	36.9 ± 0.4$^{d/x,y}$	21.8 ± 0.3$^{a/x}$	−0.1 ± 0.9$^{f/y}$	22.4 ± 0.4$^{f/x}$
	11	37.1 ± 0.3$^{d/x,y}$	20.8 ± 0.5$^{a/x}$	−0.1 ± 0.4$^{f/y}$	23.4 ± 0.5$^{f/x}$
NB + RCA	2	34.3 ± 0.3$^{a/x}$	51.5 ± 2.0$^{f/y}$	0.8 ± 0.4$^{f/x}$	9.8 ± 1.9$^{c/y}$
	3	34.0 ± 0.2$^{a/x}$	47.9 ± 0.3$^{f/y}$	−0.2 ± 0.2$^{f/x}$	6.6 ± 0.3$^{a,b/y}$
	4	33.9 ± 0.3$^{a/x}$	44.4 ± 1.6$^{e/y}$	−4.1 ± 0.4$^{c,d/x}$	4.6 ± 1.4$^{a/y}$
	5	34.1 ± 0.1$^{a/x}$	40.6 ± 1.6$^{d/y}$	−6.0 ± 1.4$^{a,b/x}$	5.4 ± 1.2$^{a,b/y}$
	6	33.9 ± 0.3$^{c/x}$	37.6 ± 0.6$^{c/y}$	−6.7 ± 0.5$^{a/x}$	7.1 ± 0.5$^{b,c/y}$
	7	34.9 ± 0.2$^{b/x}$	32.7 ± 1.0$^{b/y}$	−8.1 ± 1.0$^{a/x}$	11.4 ± 0.4$^{d/y}$
	8	34.4 ± 0.1$^{a/x}$	35.8 ± 0.8$^{c/y}$	−9.8 ± 2.6$^{a/x}$	10.9 ± 1.7$^{d/y}$
	9	36.0 ± 0.3$^{d/x}$	25.1 ± 0.3$^{a/y}$	−5.0 ± 0.2$^{a,b/x}$	16.9 ± 0.3$^{e/y}$
	10	36.9 ± 0.1$^{d/x}$	23.9 ± 0.5$^{a/y}$	−2.1 ± 0.3$^{c,d/x}$	17.7 ± 0.4$^{e/y}$
	11	37.1 ± 0.1$^{d/x}$	23.6 ± 0.5$^{a/y}$	−1.5 ± 0.2$^{c,d/x}$	17.9 ± 0.5$^{e/y}$
AP + RCA	2	34.2 ± 0.1$^{a/y}$	44.6 ± 0.7$^{d/y}$	0.9 ± 0.1$^{f/y}$	3.0 ± 0.1$^{a/y}$
	3	34.3 ± 0.1$^{a/y}$	45.1 ± 3.1$^{e/y}$	−0.0 ± 0.3$^{e,f/y}$	3.7 ± 0.1$^{a/y}$
	4	34.2 ± 0.1$^{a/y}$	45.4 ± 2.6$^{e/y}$	−3.9 ± 1.0$^{b,c/y}$	3.6 ± 0.6$^{a/y}$
	5	34.6 ± 0.1$^{a,b/y}$	41.5 ± 4.2$^{e/y}$	−7.3 ± 3.6$^{a/y}$	8.7 ± 0.3$^{c/y}$
	6	34.6 ± 0.0$^{a,b/y}$	36.1 ± 0.8$^{c/y}$	−4.0 ± 0.2$^{a,b/y}$	9.6 ± 0.7$^{c/y}$
	7	35.3 ± 0.1$^{b/y}$	32.0 ± 0.1$^{b/y}$	−5.7 ± 0.1$^{a,b/y}$	14.0 ± 0.1$^{d/y}$
	8	34.9 ± 0.1$^{c/y}$	34.9 ± 1.3$^{c/y}$	−4.9 ± 0.1$^{a,b/y}$	11.2 ± 0.9$^{d/y}$
	9	35.8 ± 0.4$^{c/y}$	28.1 ± 0.7$^{a/y}$	−4.1 ± 0.3$^{b,c/y}$	17.5 ± 0.7$^{d/y}$
	10	37.0 ± 0.0$^{d/y}$	25.3 ± 0.3$^{a/y}$	−1.8 ± 0.4$^{e,f/y}$	20.2 ± 0.3$^{f/y}$
	11	37.2 ± 0.1$^{y/d}$	24.3 ± .01$^{a/y}$	−1.2 ± 0.6$^{e,f/y}$	21.2 ± 0.0$^{f/y}$

Reported values for each starch film are means ± standard deviation (n = 3). Different letters (a, b, c, d) in the same column indicate significant differences (p < 0.05) among the different acid-base indicators for the same pH of film-forming dispersion, according to Tukey's test. Different letters (x, y) in the same column indicate significant differences ($p < 0.05$) among the different pH of film-forming dispersion for the same film formulation, according to Tukey's test.

consistent lower a* value of the AM+RCA film with respect to the AP + RCA (44.6 to 24.3) for most of the pH values, indicating a more reddish tone of this film. The NB + RCA film instead showed shifting values of a* that were similar (statistically non-dissimilar) to AM+RCA at some pH values while similar to AP + RCA at other pH values (Table 4).

The variation of the b* values for all the films showed a similar trend, with values close to zero at the extremes of the pH scale, and more negative values in the central part of the scale. This explained the visual observation of a more blue tone in all the films at a more neutral pH. Due to the higher standard error on this parameter, the statistical differences between the three films are mostly non-significant, although a consistent tendency could be observed for the NB + RCA film to show less negative b* values, indicating a less blue and more yellow tone for this polymer matrix.

A total color difference (ΔE) value >5 shows that the color changes are visually perceptible to the human eye [59]. The ΔE values showed an increasing trend with increasing pH for both AM+RCA and AP + RCA films, while the NB + RCA polymer had lower ΔE values at the beginning and then increased, with a minimum (4.5 to 5.4) around pH 4–5. The statistical analysis showed statistically different values of ΔE, indicating a relevant and appreciable change in color for all the different films, which only took place every two or three pH points, especially between 4 and 8.

At equal pH and for most of the pH values, the two films AM+RCA and AP + RCA did not show statistical differences in ΔE values, while the NB + RCA films exhibited different values, also due to the already stated different overall trend over pH. The NB + RCA films had, overall, the least change in pH-dependent ΔE and, for this reason, from a color perspective, they seem to be the least suitable to be used for the purpose of this study. Comparing the different starch type matrices AM showed a more significant difference in ΔE ($P < 0.05$) as compared to NB, and AP at different pHs. It is widely acknowledged that the color changes induced by pH are reversible. The greatest changes (ΔE) in color were observed in AP + RCA

and AM+RCA within the pH range of 6–11, indicating a significant variation in color of the indicator under slightly acidic to basic conditions, such as those found in seafood. Previous research reported that the color changes of the black carrot anthocyanins indicator were reversible upon opening the fish package. This suggests that the gaseous compounds produced could gradually dissipate, causing the indicator's color to return to its initial state [23]. This information can be taken into consideration when designing intelligent packaging materials, particularly in terms of sensing quality and gas permeability.

3.10. Photo degradation of RCAs during storage

RCAs can be degraded due to the effects of light. Hence, a photo-degradation test was performed to investigate the possible color change of the films under constant light exposure for 35 days, simulating in this way a real shelf condition in a supermarket [60]. Moreover, to examine the effect of AM content in starch films, the color parameters (L*, a*, b* and ΔE*) were measured as mentioned in Section 2.4.11. As controls, replicas of the films similar to the ones placed under light were placed in the dark (Fig. 6). The L* value was constant during the exposure time (35 days), suggesting that the color of the films did not change under visible light exposure. The AM+RCA and AP + RCA samples exhibited higher L* values than the NB + RCA during light storage conditions (Fig. 6a). During the storage time, the chroma a* values decreased, suggesting greenness, while the AP + RCA sample had the highest chroma a* values (Fig. 6b). In a previous study [60], the photo degradation of anthocyanins from jambolan fruit incorporated in chitosan/polyvinyl alcohol films demonstrated that the a* values were reduced by nearly 40 %, suggesting modifications in films containing anthocyanins. Related results were agreed with anthocyanins from acerola juice, and dry anthocyanins stabilized with nanoclays [61]. In the current study, the reduction of a* values showed that AM has the ability to protect the RCA against visible light irradiation.
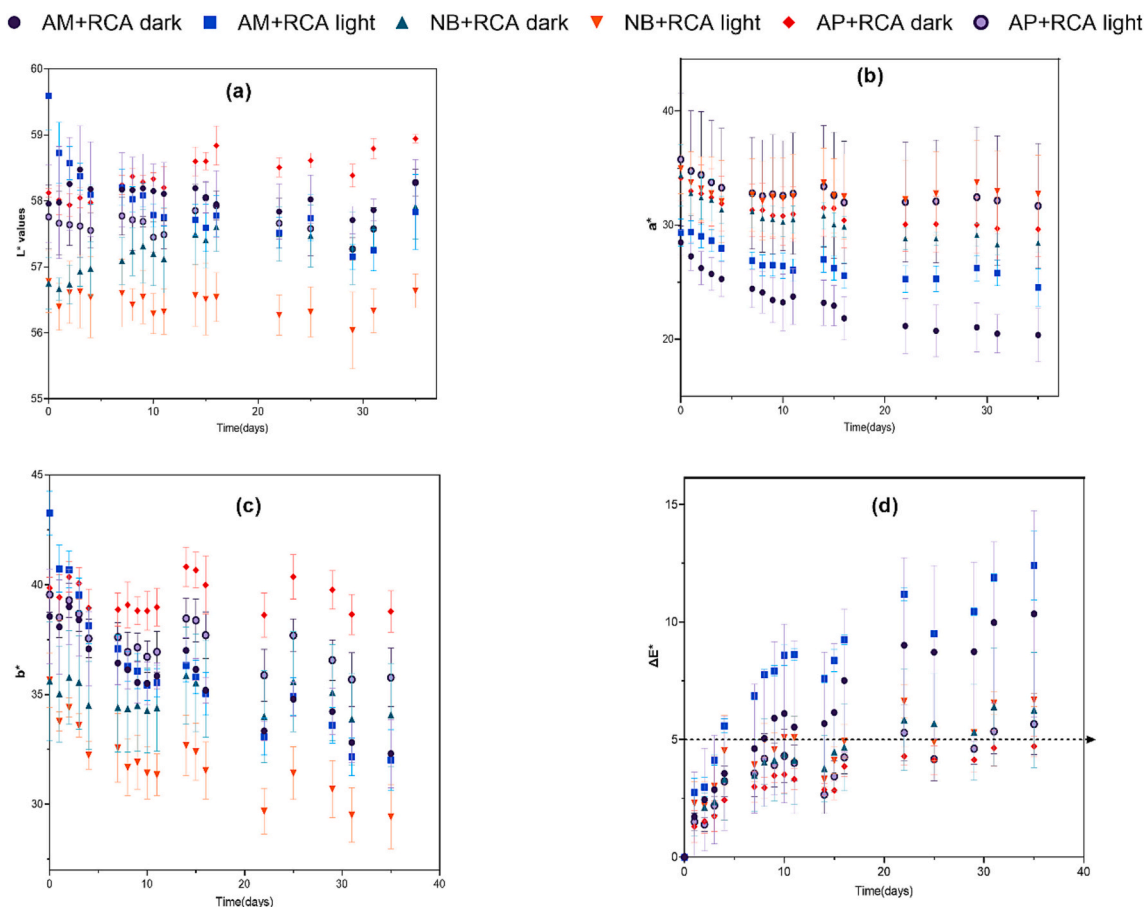
Fig. 6. Color parameter changes according to CIE Lab coordinates of films exposed to controlled visible light as a function of time: L* (a); a* (b); b* (c); and ΔE* (d) modifications. ΔE* was calculated from Eq. (8) and color parameters of each film at time zero as a reference value.

The chroma b* values decreased for all the films; however, AP + RCA and NS + RCA samples started to increase after 15 days, showing an increase in yellowness. The AM+RCA films had the highest increase in ΔE (>5), suggesting that the color change for the AM-based films can be readily sensed by the human eye compared to AP + RCA and NB + RCA during storage (Fig. 7d). There was no significant difference in the color parameters between films incubated in dark or light, which is promising for this type of responsive packaging.

Previous studies [62] reported that red cabbage anthocyanins developed higher stability compared to black anthocyanins, due to the acylated anthocyanins present in the red cabbage. The presence of aromatic acids such as sinapoyl found in the red cabbage extract has C—C double bonds. This conjugated system permits light absorbance, creating electron donors. These acyl groups are responsible for the ability to donate electrons to anthocyanin molecules, providing stability when exposed to light. The higher light stability of the acylated RCA agrees with previous studies that the acylated molecules confer higher stability to anthocyanins [38].

3.11. Release behavior of RCA

The RCA release of the films is critical for their application in real food systems. For an acetic acid food simulant [63], the release curves showed an initial burst and reached a plateau after approx. 20 min for all the films (Fig. S6). Initially, the accumulative release percentage toward diffusion equilibrium decreased with increased AM content in the film matrix. The burst release was related to the RCAs near or at the surface; RCA immobilized in the inner parts of the starch matrix take extra time to be released due to the longer pathway of diffusion [64].

The mechanism of RCAs release was evaluated based on the accumulative data; curves of M_t/M_∞ versus time were prepared and fitted to Ritger and Peppas' model (Eq. (9)) (Fig. 7a), and the relevant parameters were estimated (Table 5). A satisfying correlation with the experimental data (with R^2 between 1.00 and 0.98) was shown in the fitted model. The diffusion exponents (n) of the films were all approximately equal to 0.5, indicating that the RCA release from the films followed a Fickian diffusion mechanism (Table 5) [65], i.e., a "normal" diffusion where the flux of the RCAs is directly proportional to the diffusivity and the negative gradient of the RCAs concentration. The obtained diffusion coefficient (D) displayed that the AM films showed the least diffusion. The amylose structure plays an important role in the diffusion of solutes in the matrix, the D value decreased as amylose content increased (Table 5). This effect can be attributed to the Vh-type structure of complexed AM single helixes (Fig. 2), where anthocyanin molecules can be trapped inside these, The presence of such structures is indicated by the FTIR data (Table 2), suggesting that AM-helical crystalline aggregation is hindered by RCA, resulting in slow release compared to the NB + RCA and AP + RCA [66].

Four additional models were studied to define the release behavior of RCAs. Based on the fitting procedures, the correlation coefficients (R^2) of the five models are presented in (Fig. 7b-e). Among those models, the highest values ($R^2 = 0.98$) showed that release agreed best with a first-order model, demonstrating that the transport of RCAs in a starch matrix might be a rate limiting step. Moreover, the two models of the second-order model ($R^2 = 0.98$) and the Higuchi ($R^2 = 0.99$) models showed that the release of RCA from the starch matrix is a diffusion rather than a swelling mechanism [67].
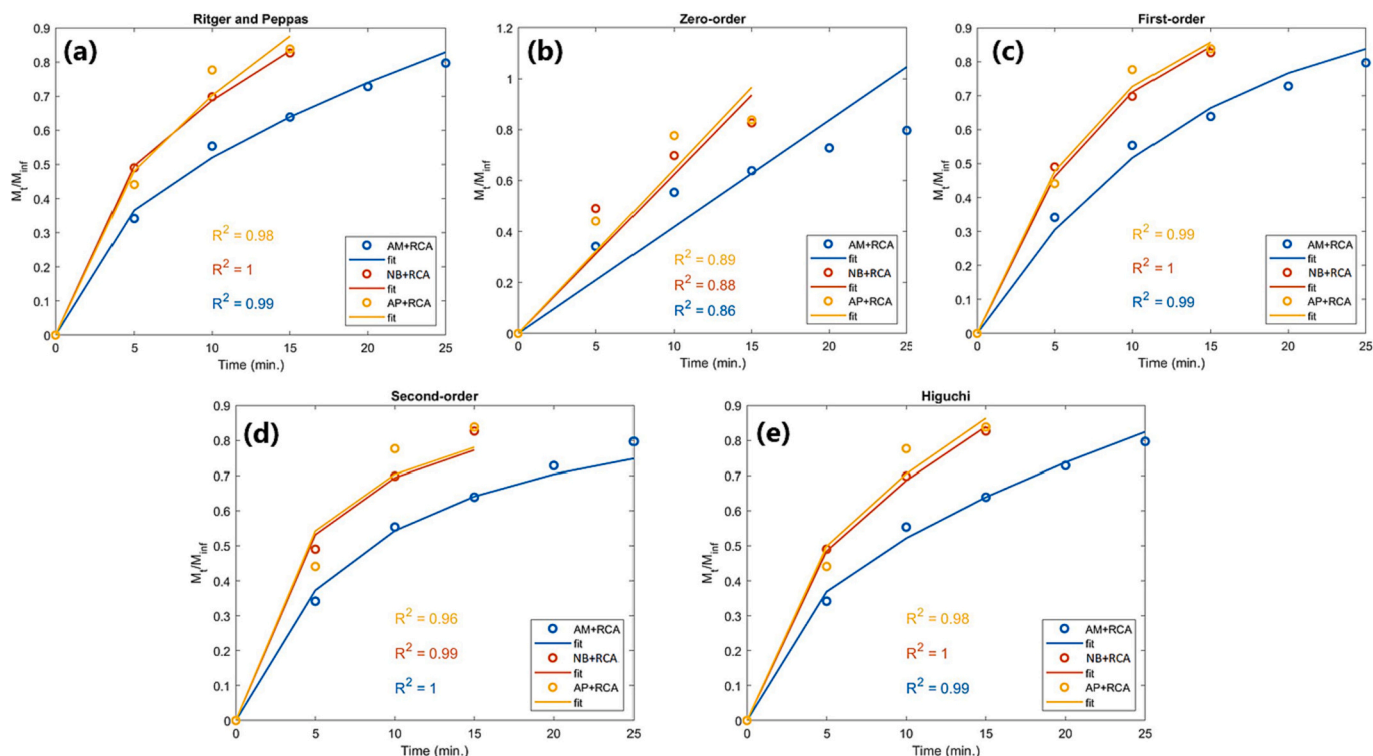
Fig. 7. Release kinetics of RCA from AP + RCA, AM+RCA and NB + RCA and modelling from the five models; a) Ritger and Peppas model, b) Zero-order model, c) First- order model, d) Second-order model, e) Higuchi- model.

Table 5
Fitting parameters of the Ritger and Peppas' model and the relative coefficient (R2) according to different models on the release mechanisms of RCAs from glucan films.

Film type	Ritger- Peppas	Zero order	R^2 First order	Second order	n Higuchi model		K	$D \times 10^{-4}$
AP + RCA	0.98	0.89	0.99	0.96	0.98	0.56	0.2001	2.0
NB + RCA	1.00	0.88	1.00	0.99	1.00	0.47	0.2322	1.8
AM+RCA	0.99	0.86	0.99	1.00	0.99	0.51	0.1612	1.6

4. Conclusion

In this study, we successfully prepared biodegradable pH-indicator films from different solid support matrices. Under the same conditions, amylose content had a significant influence on thermal, mechanical, and barrier properties. Mechanical and physical data showed that the amylose content affected the interaction with RCA. Even though RCA reduced the mechanical strength and thermal properties, it provided films with increased UV–vis blocking assets. RCA were equally dispersed in the three matrices, as demonstrated by fracture FE-SEM. AM+RCA showed better mechanical and color photo-stability than the AP and NB systems, in addition to a slower release behavior when in contact with a food simulant. FTIR data indicated a significant interaction between AM double helical structures and RCA. Based on these promising properties, AM (99 %) has demonstrated considerable potential as a new support matrix in responsive food packaging.

CRediT authorship contribution statement

Marwa Faisal: Conceptualization, Data curation, Formal analysis, Investigation, Methodology, Software, Supervision, Validation, Visualization, Writing original drafty, Writing –review &editing.
Marta Bevilacqua: Conceptualization, Data curation, Formal analysis, Investigation, Methodology, Software, Supervision, Validation, Visualization, Writing original drafty, Writing –review &editing.

Rasmus Bro: Conceptualization, Data curation, Formal analysis, Investigation, Methodology, Software, Supervision, Validation, Visualization, Writing original drafty, Writing –review &editing.
Heloisa N. Bordallo: Formal analysis, Investigation, Methodology, Software, Supervision, Validation, Visualization, Writing original drafty, Writing –review &editing, Funding acquisition.
Jacob Judas Kain Kirkensgaard: Formal analysis, Investigation, Methodology, Software, Supervision, Validation, Visualization, Writing original drafty, Writing –review &editing, Funding acquisition.
Kim H. Hebelstrup: Formal analysis, Investigation, Methodology, Software, Supervision, Validation, Visualization, Writing original drafty, Writing –review &editing.
Andreas Blennow: Conceptualization, Project administration, Funding acquisition, supervision, Writing –review &editing.

Declaration of competing interest

The authors declare that they have no known competing financial interests or personal relationships that could have appeared to influence the work reported in this paper.

Acknowledgment

Appendix A. Supplementary data

Supplementary data to this article can be found online at https://doi.org/10.1016/j.ijbiomac.2023.126250.

References

[1] L. Qiao, X. Tang, J. Dong, A feasibility quantification study of total volatile basic nitrogen (TVB-N) content in duck meat for freshness evaluation, Food Chem. 237 (2017) 1179–1185, https://doi.org/10.1016/j.foodchem.2017.06.031.

[2] C.M.L. Lires, A. Docters, C.I. Horak, Evaluation of the quality and shelf life of gamma irradiated blueberries by quarantine purposes, Radiat. Phys. Chem. 143 (2018) 79–84, https://doi.org/10.1016/j.radphyschem.2017.07.025.

[3] N. Bhargava, V.S. Sharanagat, R.S. Mor, K. Kumar, Active and intelligent biodegradable packaging films using food and food waste-derived bioactive compounds: a review, Trends Food Sci. Technol. 105 (2020) 385–401, https://doi.org/10.1016/j.tifs.2020.09.015.

[4] M. Faisal, A. Elhussieny, K.A. Ali, I. Samy, N.M. Everitt, Extraction of degradable bio polymer materials from shrimp shell wastes by two different methods, in: IOP Conference Series: Materials Science and Engineering 464, 2018, https://doi.org/10.1088/1757-899X/464/1/012004.

[5] R. Thakur, P. Pristijono, C.J. Scarlett, M. Bowyer, S.P. Singh, Q.V. Vuong, Starch-based films: major factors affecting their properties, Int. J. Biol. Macromol. 132 (2019) 1079–1089, https://doi.org/10.1016/j.ijbiomac.2019.03.190.

[6] R. Thakur, P. Pristijono, C.J. Scarlett, M. Bowyer, S.P. Singh, Q.V. Vuong, Starch-based films: major factors affecting their properties, Int. J. Biol. Macromol. (2019), https://doi.org/10.1016/j.ijbiomac.2019.03.190.

[7] D. Sagnelli, K.H. Hebelstrup, E. Leroy, A. Rolland-Sabaté, S. Guilois, J.J. K. Kirkensgaard, K. Mortensen, D. Lourdin, A. Blennow, Plant-crafted starches for bioplastics production, Carbohydr. Polym. 152 (2016) 398–408, https://doi.org/10.1016/j.carbpol.2016.07.039.

[8] A. Goldstein, G. Annor, J.L. Putaux, K.H. Hebelstrup, A. Blennow, E. Bertoft, Impact of full range of amylose contents on the architecture of starch granules*, Int. J. Biol. Macromol. 89 (2016) 305–318, https://doi.org/10.1016/j.ijbiomac.2016.04.053.

[9] U. Shah, F. Naqash, A. Gani, F.A. Masoodi, Art and science behind modified starch edible films and coatings: a review, Compr. Rev. Food Sci. Food Saf. 15 (2016) 568–580, https://doi.org/10.1111/1541-4337.12197.

[10] S. Kim, J.L. Willett, Isolation of amylose from starch solutions by phase separation, Starch/Staerke. 56 (2004) 29–36, https://doi.org/10.1002/star.200200161.

[11] M. Carciofi, A. Blennow, S.L. Jensen, S.S. Shaik, A. Henriksen, A. Buléon, P. B. Holm, K.H. Hebelstrup, Concerted suppression of all starch branching enzyme genes in barley produces amylose-only starch granules, BMC Plant Biol. 12 (2012) 1–16, https://doi.org/10.1186/1471-2229-12-223.

[12] J. Xu, D. Sagnelli, M. Faisal, A. Perzon, V. Taresco, M. Mais, C.V.L. Giosafatto, K. H. Hebelstrup, P. Ulvskov, B. Jørgensen, L. Chen, S.M. Howdle, A. Blennow, Amylose/cellulose nanofiber composites for all-natural, fully biodegradable and flexible bioplastics, Carbohydr. Polym. 253 (2021), https://doi.org/10.1016/j.carbpol.2020.117277.

[13] D. Muscat, B. Adhikari, R. Adhikari, D.S. Chaudhary, Comparative study of film forming behaviour of low and high amylose starches using glycerol and xylitol as plasticizers, J. Food Eng. 109 (2012) 189–201, https://doi.org/10.1016/j.jfoodeng.2011.10.019.

[14] M. Faisal, T. Kou, Y. Zhong, A. Blennow, High amylose-based bio composites: structures, functions and applications, Polymers. 14 (2022) 1235, https://doi.org/10.3390/polym14061235.

[15] M. Carciofi, A. Blennow, M.M. Nielsen, P.B. Holm, K.H. Hebelstrup, Barley callus: a model system for bioengineering of starch in cereals, Plant Methods 8 (2012) 1–10, https://doi.org/10.1186/1746-4811-8-36.

[16] X. Chen, X. Du, P. Chen, L. Guo, Y. Xu, X. Zhou, Morphologies and gelatinization behaviours of high-amylose maize starches during heat treatment, Carbohydr. Polym. 157 (2017) 637–642, https://doi.org/10.1016/j.carbpol.2016.10.024.

[17] J. Yang, F. Xie, W. Wen, L. Chen, X. Shang, P. Liu, Understanding the structural features of high-amylose maize starch through hydrothermal treatment, Int. J. Biol. Macromol. 84 (2016) 268–274, https://doi.org/10.1016/j.ijbiomac.2015.12.033.

[18] Y. Zhong, L. Tai, A. Blennow, L. Ding, K. Herburger, J. Qu, A. Xin, D. Guo, K. H. Hebelstrup, X. Liu, High-amylose starch: structure, functionality and applications, Crit. Rev. Food Sci. Nutr. 0 (2022) 1–23, https://doi.org/10.1080/10408398.2022.2056871.

[19] C. Tong, S. Ahmed, Y. Pang, X. Zhou, J. Bao, Fine structure and gelatinization and pasting properties relationships among starches from pigmented potatoes, Food Hydrocoll. 83 (2018) 45–52, https://doi.org/10.1016/j.foodhyd.2018.04.036.

[20] Q. Ma, L. Wang, Preparation of a visual pH-sensing film based on tara gum incorporating cellulose and extracts from grape skins, Sensors Actuators B Chem. 235 (2016) 401–407, https://doi.org/10.1016/j.snb.2016.05.107.

[21] V. Shukla, G. Kandeepan, M.R. Vishnuraj, Development of on package indicator sensor for real-time monitoring of meat quality, Vet. World 8 (2015) 393–397, https://doi.org/10.14202/vetworld.2015.393-397.

[22] V.A. Pereira, I.N.Q. de Arruda, R. Stefani, Active chitosan/PVA films with anthocyanins from Brassica oleraceae (red cabbage) as time-temperature indicators for application in intelligent food packaging, Food Hydrocoll. 43 (2015) 180–188, https://doi.org/10.1016/j.foodhyd.2014.05.014.

[23] F. Ebrahimi Tirtashi, M. Moradi, H. Tajik, M. Forough, P. Ezati, B. Kuswandi, Cellulose/chitosan pH-responsive indicator incorporated with carrot anthocyanins for intelligent food packaging, Int. J. Biol. Macromol. 136 (2019) 920–926, https://doi.org/10.1016/j.ijbiomac.2019.06.148.

[24] P. Ezati, J.W. Rhim, pH-responsive pectin-based multifunctional films incorporated with curcumin and sulfur nanoparticles, Carbohydr. Polym. 230 (2020), 115638, https://doi.org/10.1016/j.carbpol.2019.115638.

[25] S. Mohammadalinejhad, H. Almasi, M. Moradi, Immobilization of Echium amoenum anthocyanins into bacterial cellulose film: a novel colorimetric pH indicator for freshness/spoilage monitoring of shrimp, Food Control 113 (2020), 107169, https://doi.org/10.1016/j.foodcont.2020.107169.

[26] U.K. Ibrahim, I.I. Muhammad, R.M. Salleh, The effect of pH on color behavior of Brassica oleracea anthocyanin, J. Appl. Sci. 11 (2011) 2406–2410, https://doi.org/10.3923/jas.2011.2406.2410.

[27] M.A. Knapp, D.F. dos Santos, D. Pilatti-Riccio, V.G. Deon, G.H.F. dos Santos, V. Z. Pinto, Yerba mate extract in active starch films: mechanical and antioxidant properties, J. Food Process. Preserv. 43 (2019) 1–12, https://doi.org/10.1111/jfpp.13897.

[28] J. Xu, A. Blennow, X. Li, L. Chen, X. Liu, Gelatinization dynamics of starch in dependence of its lamellar structure, crystalline polymorphs and amylose content, Carbohydr. Polym. 229 (2020), 115481, https://doi.org/10.1016/j.carbpol.2019.115481.

[29] J. Lee, R.W. Durst, R.E. Wrolstad, Determination of total monomeric anthocyanin pigment content of fruit juices, beverages, natural colorants, and wines by the pH differential method: collaborative study, J. AOAC Int. 88 (2005) 1269–1278, https://doi.org/10.1093/jaoac/88.5.1269.

[30] X. Zhai, J. Shi, X. Zou, S. Wang, C. Jiang, J. Zhang, X. Huang, W. Zhang, M. Holmes, Novel colorimetric films based on starch/polyvinyl alcohol incorporated with roselle anthocyanins for fish freshness monitoring, Food Hydrocoll. 69 (2017) 308–317, https://doi.org/10.1016/j.foodhyd.2017.02.014.

[31] S.M. Ojagh, M. Rezaei, S.H. Razavi, S.M.H. Hosseini, Development and evaluation of a novel biodegradable film made from chitosan and cinnamon essential oil with low affinity toward water, Food Chem. 122 (2010) 161–166, https://doi.org/10.1016/j.foodchem.2010.02.033.

[32] L. Mariniello, C.V.L. Giosafatto, P. Di Pierro, A. Sorrentino, R. Porta, Swelling, mechanical, and barrier properties of albedo-based films prepared in the presence of phaseolin cross-linked or not by transglutaminase, Biomacromolecules. 11 (2010) 2394–2398, https://doi.org/10.1021/bm100566j.

[33] C. Holland, A. Perzon, P.R.C. Cassland, J.P. Jensen, B. Langebeck, O.B. Sørensen, E. Whale, D. Hepworth, R. Plaice-Inglis, Ø. Moestrup, P. Ulvskov, B. Jørgensen, Nanofibers produced from agro-industrial plant waste using entirely enzymatic pretreatments, Biomacromolecules. 20 (2019) 443–453, https://doi.org/10.1021/acs.biomac.8b01435.

[34] J. Liu, H. Yong, Y. Liu, Y. Qin, J. Kan, J. Liu, Preparation and characterization of active and intelligent films based on fish gelatin and haskap berries (Lonicera caerulea L.) extract, Food Packag. Shelf Life 22 (2019) 100417, https://doi.org/10.1016/j.fpsl.2019.100417.

[35] S. Wold, M. Sjostrom, PLS-regression: A Basic Tool of Chemometrics, 2001, pp. 109–130.

[36] M.P. Arrieta, M. Castro-lo, E. Rayo, L.F. Barral-losada, J. Manuel, Plasticized Poly (lactic acid) − Poly(hydroxybutyrate) (PLA − PHB) Blends Incorporated with Catechin Intended for Active Food- Packaging Applications, 2014.

[37] J. Liu, H. Wang, M. Guo, L. Li, M. Chen, S. Jiang, X. Li, S. Jiang, Food Hydrocolloids Extract from Lycium ruthenicum Murr. Incorporating κ-carrageenan colorimetric film with a wide pH – sensing range for food freshness monitoring, Food Hydrocoll. 94 (2019) 1–10, https://doi.org/10.1016/j.foodhyd.2019.03.008.

[38] L. Prietto, T.C. Mirapalhete, V.Z. Pinto, J.F. Hoffmann, N.L. Vanier, L.T. Lim, A. R. Guerra Dias, E. da Rosa Zavareze, pH-sensitive films containing anthocyanins extracted from black bean seed coat and red cabbage, LWT Food Sci. Technol. 80 (2017) 492–500, https://doi.org/10.1016/j.lwt.2017.03.006.

[39] G.F. Nogueira, C.T. Soares, R. Cavasini, F.M. Fakhouri, R.A. de Oliveira, Bioactive films of arrowroot starch and blackberry pulp: physical, mechanical and barrier properties and stability to pH and sterilization, Food Chem. 275 (2019) 417–425, https://doi.org/10.1016/j.foodchem.2018.09.054.

[40] Y. Kumar, S. Prateek, S. Praneeta, P.P. Prabhakaran, V.K. Tanwar, Bio-plastics: a perfect tool for eco-friendly food packaging: a review, J. Food Product Dev. Packag. 1 (2014) 1–6, www.jakraya.com/journal/jfpdp.

[41] Y. Qin, Y. Liu, H. Yong, J. Liu, X. Zhang, J. Liu, Preparation and characterization of active and intelligent packaging films based on cassava starch and anthocyanins from Lycium ruthenicum Murr, Int. J. Biol. Macromol. 134 (2019) 80–90, https://doi.org/10.1016/j.ijbiomac.2019.05.029.

[42] M.C. Silva-Pereira, J.A. Teixeira, V.A. Pereira-Júnior, R. Stefani, Chitosan/corn starch blend films with extract from Brassica oleraceae (red cabbage) as a visual indicator of fish deterioration, Lwt. 61 (2015) 258–262, https://doi.org/10.1016/j.lwt.2014.11.041.

[43] Y. Chai, M. Wang, G. Zhang, Interaction between amylose and tea polyphenols modulates the postprandial glycemic response to high-amylose maize starch, J. Agric. Food Chem. 61 (2013) 8608–8615, https://doi.org/10.1021/jf402821r.

[44] H. Xu, L. Chen, Z. Xu, D.J. McClements, H. Cheng, C. Qiu, J. Long, H. Ji, M. Meng, Z. Jin, Structure and properties of flexible starch-based double network composite films induced by dopamine self-polymerization, Carbohydr. Polym. 299 (2023), 120106, https://doi.org/10.1016/j.carbpol.2022.120106.

[45] H. Yong, X. Wang, R. Bai, Z. Miao, X. Zhang, J. Liu, Development of antioxidant and intelligent pH-sensing packaging films by incorporating purple-fleshed sweet potato extract into chitosan matrix, Food Hydrocoll. 90 (2019) 216–224, https://doi.org/10.1016/j.foodhyd.2018.12.015.

[46] E. Basiak, A. Lenart, F. Debeaufort, Effect of starch type on the physico-chemical properties of edible films, Int. J. Biol. Macromol. 98 (2017) 348–356, https://doi.org/10.1016/j.ijbiomac.2017.01.122.

[47] J. Dong, S. Li, J. Zhang, A. Liu, J. Ren, Thermal degradation of cyanidin-3-O-glucoside: mechanism and toxicity of products, Food Chem. 370 (2022), https://doi.org/10.1016/j.foodchem.2021.131018.

[48] X. Cai, X. Du, D. Cui, X. Wang, Z. Yang, G. Zhu, Improvement of stability of blueberry anthocyanins by carboxymethyl starch/xanthan gum combinations microencapsulation, Food Hydrocoll. 91 (2019) 238–245, https://doi.org/10.1016/j.foodhyd.2019.01.034.

[49] A. Jiménez, M.J. Fabra, P. Talens, A. Chiralt, Effect of sodium caseinate on properties and ageing behaviour of corn starch based films, Food Hydrocoll. 29 (2012) 265–271, https://doi.org/10.1016/j.foodhyd.2012.03.014.

[50] L. Lin, D. Guo, L. Zhao, X. Zhang, J. Wang, F. Zhang, C. Wei, Comparative structure of starches from high-amylose maize inbred lines and their hybrids, Food Hydrocoll. 52 (2016) 19–28, https://doi.org/10.1016/j.foodhyd.2015.06.008.

[51] P. Jha, Functional properties of starch-chitosan blend bionanocomposite films for food packaging: the influence of amylose-amylopectin ratios, J. Food Sci. Technol. 58 (2021) 3368–3378, https://doi.org/10.1007/s13197-020-04908-2.

[52] M.M. Góes, B.M. Simões, F. Yamashita, S. Mali de Oliveira, G.M. de Carvalho, Plasticizers' effect on pH indicator film based on starch and red grape skin extract for monitoring fish freshness, Packag. Technol. Sci. (2023) 1–13, https://doi.org/10.1002/pts.2719.

[53] L. Godbillot, P. Dole, C. Joly, B. Rogé, M. Mathlouthi, Analysis of water binding in starch plasticized films, Food Chem. 96 (2006) 380–386, https://doi.org/10.1016/j.foodchem.2005.02.054.

[54] F.M. Pelissari, M.M. Andrade-Mahecha, P.J. do A. Sobral, F.C. Menegalli, Comparative study on the properties of flour and starch films of plantain bananas (Musa paradisiaca), Food Hydrocoll. 30 (2013) 681–690, https://doi.org/10.1016/j.foodhyd.2012.08.007.

[55] S. Liu, T.Z. Yuan, X. Wang, M. Reimer, C. Isaak, Y. Ai, Behaviors of starches evaluated at high heating temperatures using a new model of Rapid Visco Analyzer – RVA 4800, Food Hydrocoll. 94 (2019) 217–228, https://doi.org/10.1016/j.foodhyd.2019.03.015.

[56] M.A. Bertuzzi, M. Armada, J.C. Gottifredi, Physicochemical characterization of starch based films, J. Food Eng. 82 (2007) 17–25, https://doi.org/10.1016/j.jfoodeng.2006.12.016.

[57] N. Yang, W. Gao, F. Zou, H. Tao, L. Guo, B. Cui, L. Lu, Y. Fang, P. Liu, Z. Wu, The relationship between molecular structure and film-forming properties of thermoplastic starches from different botanical sources, Int. J. Biol. Macromol. 230 (2023), https://doi.org/10.1016/j.ijbiomac.2022.123114.

[58] I. Leceta, P. Guerrero, K. De Caba, Functional properties of chitosan-based films, Carbohydr. Polym. 93 (2013) 339–346, https://doi.org/10.1016/j.carbpol.2012.04.031.

[59] S. Tassanawat, A. Phandee, R. Magaraphan, M. Nithitanakul, H. Manuspiya, pH-Sensitive PP/clay nanocomposites for beverage smart packaging, in: Proceedings of the 2nd IEEE International Conference on Nano/Micro Engineered and Molecular Systems, IEEE NEMS 2007, 2007, pp. 478–482, https://doi.org/10.1109/NEMS.2007.352062.

[60] B. Merz, C. Capello, G.C. Leandro, D.E. Moritz, A.R. Monteiro, G.A. Valencia, A novel colorimetric indicator film based on chitosan, polyvinyl alcohol and anthocyanins from jambolan (Syzygium cumini) fruit for monitoring shrimp freshness, Int. J. Biol. Macromol. 153 (2020) 625–632, https://doi.org/10.1016/j.ijbiomac.2020.03.048.

[61] Y. Alexandra, R. Gaviria, N. Stefanía, N. Palencia, C. Capello, Nanostructured pH-indicator films based on cassava starch, laponite, and jambolan (*Syzygium cumini*), in: Fruit Manufactured by Thermo-Compression 2000208, 2021, pp. 1–11, https://doi.org/10.1002/star.202000208.

[62] F.C. Stintzing, A.S. Stintzing, R. Carle, B. Frei, R.E. Wrolstad, Color and antioxidant properties of cyanidin-based anthocyanin pigments, J. Agric. Food Chem. 50 (2002) 6172–6181, https://doi.org/10.1021/jf0204811.

[63] European Union, Commission Regulation (EU) No 10/2011 of 14 January 2011, Off. J. Eur. Union (2011) 1–89. https://eur-lex.europa.eu/LexUriServ/LexUriServ.do?uri=OJ:L:2011:012:0001:0089:EN:PDF.

[64] C. Wu, Y. Li, J. Sun, Y. Lu, C. Tong, L. Wang, Z. Yan, J. Pang, Novel konjac glucomannan films with oxidized chitin nanocrystals immobilized red cabbage anthocyanins for intelligent food packaging, Food Hydrocoll. 98 (2020), 105245, https://doi.org/10.1016/j.foodhyd.2019.105245.

[65] S. Wang, L. Copeland, Effect of acid hydrolysis on starch structure and functionality: a review, Crit. Rev. Food Sci. Nutr. 55 (2015) 1079–1095, https://doi.org/10.1080/10408398.2012.684551.

[66] L. Kong, G.R. Ziegler, Molecular encapsulation of ascorbyl palmitate in preformed V-type starch and amylose, Carbohydr. Polym. 111 (2014) 256–263, https://doi.org/10.1016/j.carbpol.2014.04.033.

[67] K. Derakhshandeh, M. Erfan, S. Dadashzadeh, Encapsulation of 9-nitrocampto-thecin, a novel anticancer drug, in biodegradable nanoparticles: factorial design, characterization and release kinetics, Eur. J. Pharm. Biopharm. 66 (2007) 34–41, https://doi.org/10.1016/j.ejpb.2006.09.004.